ORNL/TM--8504

DE83 003349

ORNL/TM-8504
Dist. Category UC-20d

Contract No. W-7405-eng-26

Engineering Physics Division

STREAMING OF 14-MEV NEUTRONS THROUGH AN IRON DUCT: COMPARISON OF MEASURED NEUTRON AND GAMMA-RAY ENERGY SPECTRA WITH RESULTS CALCULATED USING THE MONTE CARLO CODE MCNP*

R. T. Santoro
J. M. Barnes[+]
P. D. Soran[§]
R. G. Alsmiller, Jr.

*Submitted for Journal publication

[+]UCC-ND Computer Sciences Division

[§]Los Alamos National Laboratory

This Work Sponsored by
Office of Fusion Energy
U.S. Department of Energy

NOTICE This document contains information of a preliminary nature. It is subject to revision or correction and therefore does not represent a final report.

Date Published - November 1982

OAK RIDGE NATIONAL LABORATORY
Oak Ridge, Tennessee 37830
operated by
UNION CARBIDE CORPORATION
for the
DEPARTMENT OF ENERGY

TABLE OF CONTENTS

STREAMING OF 14-MeV NEUTRONS THROUGH AN IRON DUCT - COMPARISON OF MEASURED NEUTRON AND GAMMA RAY ENERGY SPECTRA WITH RESULTS CALCULATED USING THE MONTE CARLO CODE MCNP*

R. T. Santoro, J. M. Barnes, P. D. Soran,** and R. G. Alsmiller, Jr.

Oak Ridge National Laboratory, Oak Ridge, Tennessee 37830

ABSTRACT

Neutron and gamma-ray energy spectra resulting from the streaming of 14 MeV neutrons through a 0.30-m-diameter duct (length-to-diameter ratio = 2.83) have been calculated using the Monte Carlo code MCNP. The calculated spectra are compared with measured data and data calculated previously using a combination of discrete ordinates and Monte Carlo methods. Comparisons are made at twelve detector locations on and off the duct axis for neutrons with energies above 850 keV and for gamma rays with energies above 750 keV. The neutron spectra calculated using MCNP agree with the measured data within ~5 to ~50%, depending on detector location and neutron energy. Agreement with the measured gamma-ray spectra is also within ~5 to ~50%. The spectra obtained with MCNP are also in favorable agreement with the previously calculated data and were obtained with less calculational effort.

I. INTRODUCTION

Numerous analytic studies have been made to estimate the effects of radiation streaming on fusion reactor and reactor component performance.[1-7] Fusion reactors will contain numerous ducts and other penetrations in the blanket-shield assembly that are required for vacuum pumping, rf heating, neutral beam injection, diagnostics, etc. The 14.5 MeV neutrons produced in the plasma from deuterium-tritium (DT) reactions along with low-energy neutrons and gamma rays produced from the interactions of these neutrons in the materials surrounding the plasma will stream through the penetrations and produce excess radiation levels outside the reactor shield. This radiation will lead to intolerable levels of nuclear heating, radiation damage, and induced activation in critical reactor components that will impact the performance, maintenance, and replacement of the components.

The effects of radiation streaming on the design of fusion reactors has prompted the need for verifying the radiation transport methods and nuclear data being used in the analysis of these types of problems. Since there are no operating neutron-producing fusion reactors in existence, measured data to provide the verification must be obtained using accelerators to produce ~14 MeV neutrons and measurements must be made using representative, or prototypic, experimental configurations. A program of integral experiments is underway at the Oak Ridge National Laboratory to obtain measured data from ~14 MeV neutrons streaming through ducts having characteristics typical of those found in fusion reactors.

In this paper, measured neutron and gamma-ray energy spectra resulting from the streaming of ~14 MeV neutrons through a 0.30-m-diameter iron duct having a length-to-diameter (L/D) ratio of 2.83 are compared with calculated spectra obtained using the Monte Carlo code MCNP.[8] In a previous paper, hereinafter referred to as Ref. 9, the measured neutron and gamma-ray spectra were compared with spectra calculated using discrete ordinates methods and also with spectra calculated using a combination of discrete ordinates and Monte Carlo radiation transport methods.

The spectra calculated using only discrete ordinates radiation transport codes in a sequence that accounts for the uncollided, first collision, and multiply collided neutron contributions to the flux at the detector[10-12] were generally in poor agreement with the measured data at neutron energies >10 MeV at the off-axis detectors. The radiation transport was performed using multigroup formatted cross section data with the neutron and gamma-ray scattering angular distributions represented by Legendre polynomial expansions. In these calculations, a 53-neutron, 21-gamma-ray cross section library obtained by collapsing the 171 neutron, 36-gamma-ray VITAMIN C data library (ENDF/B-IV) was used.[13] The neutron and gamma-ray scattering was approximated using P_3 expanded angular distributions.

The disagreement between the measured and calculated neutron spectra was due to the inadequacy of the P_3 expanded neutron scattering angular distributions for predicting the single scattering of energetic (>10 MeV) neutrons from the iron duct to the off-axis detectors. Neutron elastic and inelastic single scattering is very forwardly peaked at neutron energies above 10 MeV and a P_3 expansion results in a poor fit to the scattering angular distributions.

To resolve the disagreement, the spectra were also calculated using a combination of discrete ordinates (with multigroup formatted cross section data) and Monte Carlo (with continuous cross section data) radiation transport methods. The Monte Carlo code PXMORSE[14] that performs the transport of neutrons by sampling from cross sections that are continuous in energy rather than averaged over multigroup energy intervals was used.

The calculated neutron spectra were obtained by removing the single scattered neutron contributions to the flux from the discrete ordinates calculation and adding the same data calculated by the Monte Carlo method. The uncollided and multiply collided neutron flux contributions calculated in the discrete ordinates sequence were retained. The comparisons between the measured and calculated spectra were considerably improved at all detector locations. The results obtained suggested that radiation streaming should be analyzed using transport codes that utilize continuous cross section data or by the networking of codes that use both multigroup and continuous cross section data in order to account for neutron single scattering. The latter approach, however, requires extensive data management and long computer running times.

The experiment described in Ref. 9 was reanalyzed considering the first option and using the Monte Carlo code MCNP.[8] MCNP is a general purpose, continuous-energy, generalized geometry, time-dependent, coupled neutron-photon Monte Carlo transport code. Pointwise cross section data are treated in considerable detail in energy grids that are tailored for each isotope in the cross section data libraries.[8] The angular distributions for elastic and inelastic scattering are also described on a fine grid of incident neutron energies and linear interpolation methods are used to obtain the angular distribution of the scattered neutron versus incoming neutron energy. The angular distribution of the outgoing particle is then sampled in a continuous fashion.

A brief description of the experiment is given in Sec. II. The details of the MCNP calculation, including the modeling of the experiment, neutron source descriptions, and the nuclear data are given in Sec. III. The calculated neutron and gamma ray spectra are compared with the measured data and those obtained in Ref. 9 in Sec. IV.

II. DESCRIPTION OF THE EXPERIMENT

The experimental facility that was constructed for the measurements reported here is described in Refs. 9, 15, and 16, so only those details necessary for interpreting the results calculated here are given. An electrostatic generator is used to accelerate deuterons to a kinetic energy of 250 keV. The deuterons are directed through a drift tube onto a 4 mg/cm^2 thick titanium-tritide target to produce neutrons via the DT fusion reaction. The tritium target is enclosed in a cylindrical re-entrant iron can having an inner diameter of 0.30 m and a wall thickness of 0.075 m. The iron can tailors the neutron spectrum and makes it characteristic of that incident on the first wall of a fusion reactor.[15] The iron duct through which the neutrons stream forms an extension of the iron can. The wall thickness and inner diameter of the duct are the same as the iron source can. The duct extends 0.85 m from the tritium

target (neutron source) and has a L/D ratio, measured from the target to the mouth of the duct, of 2.83. The iron source can-duct assembly is enclosed in a concrete shield-support structure. The concrete has a thickness of 1 m in all directions perpendicular to the deuteron beam-target-duct axis making it effective as a biological shield and for reducing the neutron and gamma-ray background radiation levels in the vicinity of the detectors.

The neutron and gamma-ray spectra were measured at various locations on and off the duct axis and at various source-to-detector distances using an NE-213 liquid scintillator. The spectra were normalized to the absolute neutron yield from the target which was determined using the associated particle method.[16] Pulse-shape-discrimination techniques were used to separate neutron and gamma-ray induced events in the detector. Neutron spectra were measured for neutrons with energies above 850 keV and gamma-ray spectra were measured for photons with energies greater than 750 keV.

III. DETAILS OF THE CALCULATIONS

The MCNP calculations were carried out using the two-dimensional model of the experimental configuration shown in Fig. 1. The concrete shield-support structure, source-can-iron-duct assembly, and the concrete-wall-thermal neutron shield located behind the detectors were modeled in r-z geometry with cylindrical symmetry about the duct axis. The neutron and neutron-induced gamma-ray fluences were calculated using point estimators.

Neutrons produced in the DT reaction have an angle-energy dependence that must be accounted for in the calculations to assure that the measured and calculated neutron and gamma-ray spectra are compared to the same neutron source. The neutron and gamma-ray spectra were calculated with MCNP in two steps: first, by sampling from neutrons emitted from the target into the polar angular interval between 0 and 40° (forward calculation) and then by sampling from neutrons emitted into the angular interval between 40 and 180° (backward calculation). The probabilities for the emission of neutrons into these angular intervals from the reactions of 250 keV deuterons in a 4 mg/cm^2-thick titanium-tritide target are given as a function of neutron energy in Table I.

MCNP includes options for sampling from the neutron source in both angle and energy. In this work, source neutrons were angularly biased by specifying the probability for neutron emission into cones of fixed size. For the forward emitted neutrons, the cone angle, θ, measured between the cone axis and the cone edge, was 40°. For the backward emitted neutrons, the cone angle was 140° (measured from the negative z-axis). Particles were then sampled uniformly in the cone, $\cos\theta \leq w \leq 1$, with probability $p = 1$ (w is the direction cosine wth the z axis) and were assumed to be emitted from the target with an isotropic distribution in the cone. Neutrons having direction cosines u and v with the x and y axes, respectively, were not angularly biased.

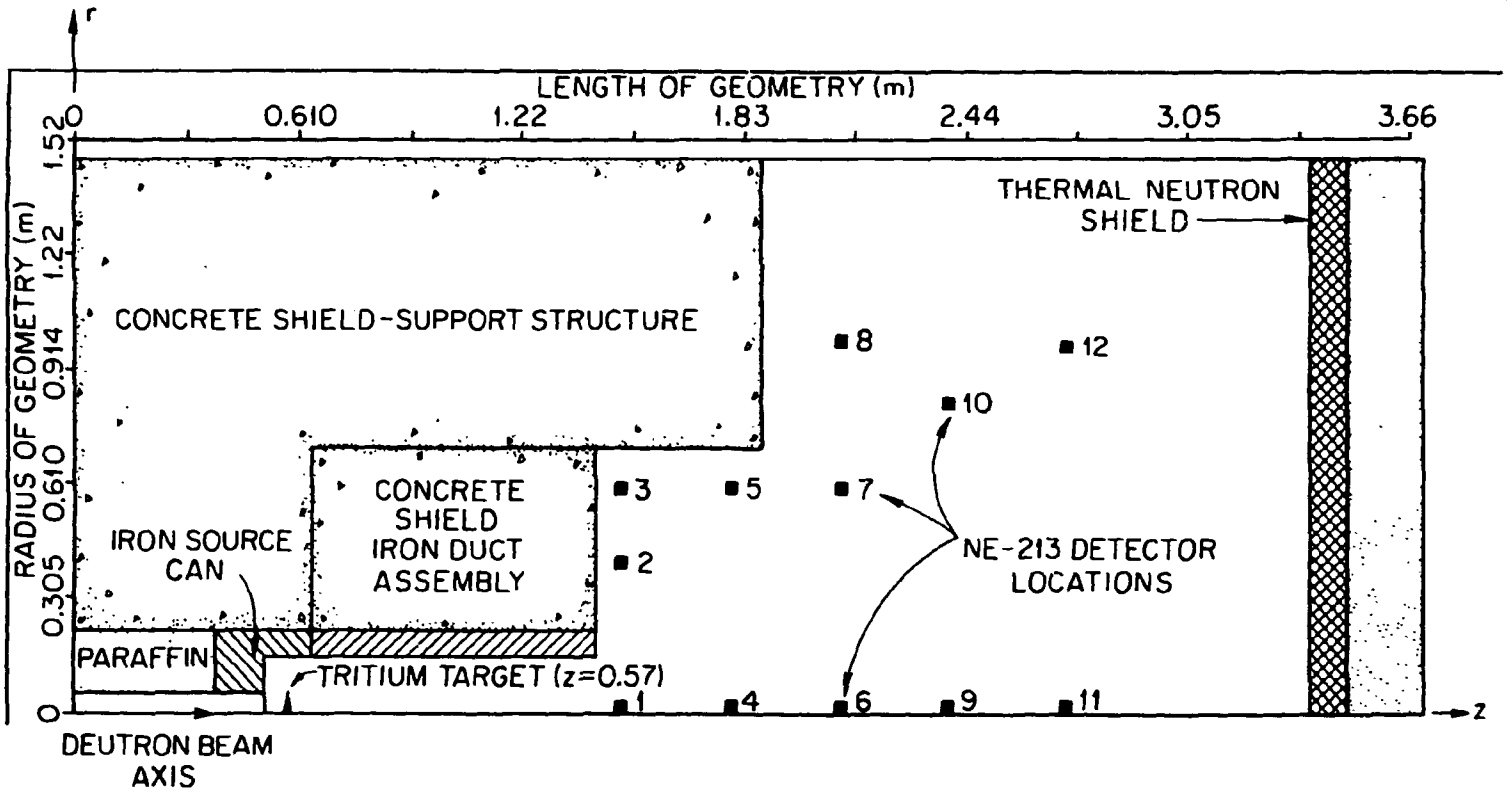

Fig. 1. Two-dimensional calculational model of the experimental configuration.

Table I

Angle-Energy Dependence for Neutrons Emitted
from the $T(D,n)^4He$ Reaction

(Deuteron Energy = 250 keV)

Energy Interval (MeV)	Angular Interval 0-40°	40-180°
14.92-15.68	0.0130	
14.55-14.92	0.0902	0.0697
14.19-14.55	0.0168	0.2460
13.80-14.19		0.2913
13.50-13.80		0.2088
12.84-13.50		0.0642
Total	0.1200	0.8800

The forward and backward emitted source neutrons were assigned weights, W, according to the relation

$$W = W' (1-\cos\theta)/2p \tag{1}$$

where W′ is the unbiased source particle weight. For the forward emitted source particles, W_f = 0.1170 W′. For the backward emitted source particles, W_b = 0.8830 W′. Since W′ = 1, unit particle weight in the combined forward and backward analyses is preserved. ($W_f + W_b = 1$).

The source neutron energies were obtained by sampling uniformly within the energy intervals given in Table I according to the specified probabilities. To account for the anisotropy of particle emission into each cone, the probabilities for neutron production in the specified angle-energy intervals, $P(\Delta E,\Delta\theta)$, were weighted using a solid angle factor given by

$$P_w(\Delta E,\Delta\theta) = \frac{2P(\Delta E,\Delta\theta)}{\int_{\theta_1}^{\theta_2} \sin\theta' d\theta'} = \frac{P(\Delta E,\Delta\theta)}{W_i} \quad ,i=f,b \tag{2}$$

where $P_w(\Delta E,\Delta\theta)$ is the solid angle weighted probability for neutrons in the energy interval ΔE and angular interval $\Delta\theta$, where P(ΔE, 0-40°) = 0.1200 and P(ΔE, 40°-180°) = 0.8800 as shown in Table I. Thus, to maintain the weighting according to the angle-energy dependence, the weights W_f and W_b are multiplied by the appropriate $P_w(\Delta E,\Delta\theta)$ given by Eq. (2).

The neutron flux at each detector position was obtained by combining the neutron fluxes calculated in the forward and backward analyses according to the relation

$$\phi_T^n(E) = \phi_{FU}^n(E) + \phi_{FC}^n(E) + \phi_{BC}^n(E) \tag{3}$$

where

ϕ_T^n(E) = the total neutron flux at energy E per source neutron,

ϕ_{FU}^n(E) = the uncollided neutron flux at energy E per source neutron from neutrons emitted in the forward direction,

ϕ_{FC}^n(E) = the collided neutron flux at energy E per source neutron from neutrons emitted in the forward direction, and

ϕ_{BC}^n(E) = the collided neutron flux at energy E per source neutron from neutrons emitted in the backward direction.

There is no contribution to the uncollided neutron flux at the detectors from neutrons emitted in the backward directions.

The gamma-ray spectra at each detector location was obtained according to the relation

$$\phi_T^\gamma(E) = \phi_F^\gamma(E) + \phi_B^\gamma(E) \tag{4}$$

where

ϕ_T^γ = the total gamma-ray flux at energy E per source neutron,

ϕ_F^γ = the gamma-ray flux at energy E per source neutron produced by neutrons emitted in the forward directions, and

ϕ_B^γ = gamma-ray flux at energy E per source neutron produced by neutrons emitted in the backward directions.

Russian Roulette and particle splitting were used to reduce the variance of the calculated neutron and gamma-ray fluxes.

The MCNP calculations were carried out using ENDF/B-V transport cross sections for the compositions of the materials given in Table II.

IV. DISCUSSION OF RESULTS

The neutron energy spectra calculated using the MCNP code are compared with the measured spectra as a function of detector location relative to the duct in Figs. 2-6. Also shown in the figures are the spectra calculated in Ref. 9 using discrete ordinates plus Monte Carlo methods. These data are included for the purpose of comparing the calculated spectra obtained using two different radiation transport methods.

In the figures, the solid curves show the measured spectra, the solid circles are the MCNP results, and the open squares are the calculated data from Ref. 9. The two solid curves at each detector location represent a 68% confidence interval in the measured spectra. The uncertainty is introduced by the unfolding of the neutron spectra from the measured pulse-height distributions.[17] The calculated data have been smoothed by convoluting the neutron flux per unit energy with an energy-dependent Gaussian response function having a width determined from

$$R_n = [300 + 800/E_n]^{1/2} \quad (5)$$

where R_n is the full width at half-maximum (in percent) of the NE-213 detector resolution to neutrons of energy E_n. The neutron flux was binned into energy intervals having the same widths as those used in the calculations in Ref. 9 so the smoothing of the MCNP results were carried out in the same manner as in Ref. 9. The error bars shown on the MCNP data represent plus and minus one standard deviation in the estimated spectra. Where no error bars are shown, they are of the order of the size of the circles. The MCNP code was run for both the forward and backward neutron source distributions with a sufficient sample size to obtain $\pm 5\%$ standard deviation in the unsmoothed neutron flux in the energy intervals above 10 MeV. The error bars on the data plotted in Figs. 2-6 were obtained by separately smoothing the upper and lower bounds of the neutron flux determined from the statistical variation in the flux in each energy bin.

The neutron spectra in Figs. 2-6 are compared for neutron energies above 850 keV. For the purposes of displaying the data, some of the spectra have been multiplied by factors of 10^{-n}, $n = 1,2$, etc. The actual magnitude of the data may be restored by multiplying the neutron flux per unit energy by the appropriate factor of 10^n. The coordinates of the detector locations are given in the figures and also summarized in Table III. The source-to-detector distance specified in each figure is along the z-axis from the target to the centerline of the detector.

Examination of Figs. 2-6 reveals that the neutron spectra calculated using the MCNP code are generally in good agreement with the measured spectra at all detector locations. Also, these data are in very favorable agreement with the spectra calculated in Ref. 9. For the cases where the detector is on

Table II

Composition of Materials

Element	Composition (Atom/cm·Barn)			
	Concrete	Air	Iron	SS-304
H	7.86-3*			
N		3.64-5		
O	4.39-2	9.74-6		
Na	1.05-3			
Mg	1.40-4			
Al	2.39-3			
Si	1.58-2			
K	6.90-4			
Ca	2.92-3			
Cr				1.77-2
Mn				1.77-3
Fe	3.10-4		8.48-2	6.02-2
Ni				7.83-3

*Read as 7.86×10^{-3}

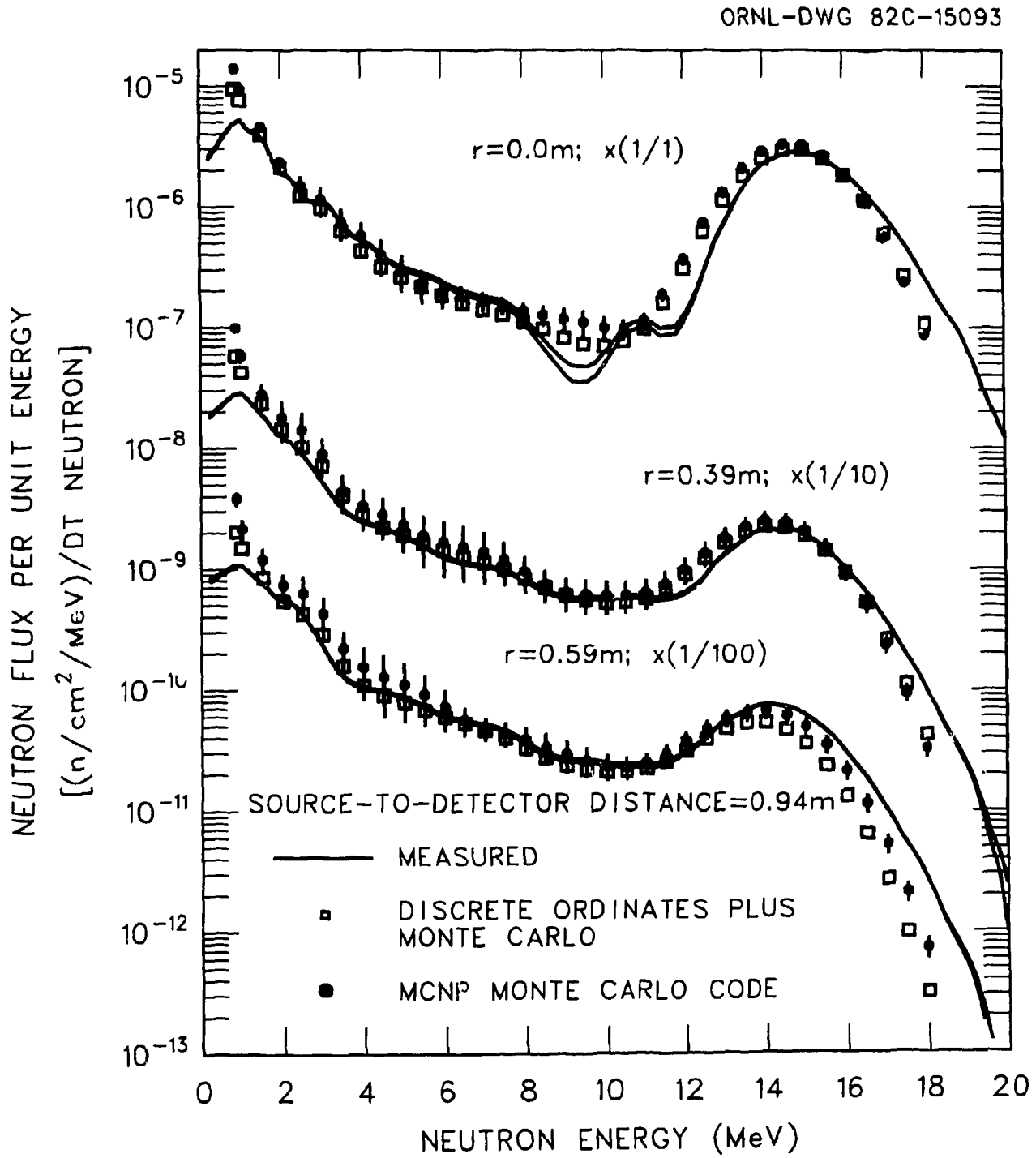

Fig. 2. Neutron flux per unit energy versus neutron energy for the detector at a distance along the z-axis of 0.94 m and at radial distances of 0.0, 0.39, and 0.59 m from the axis.

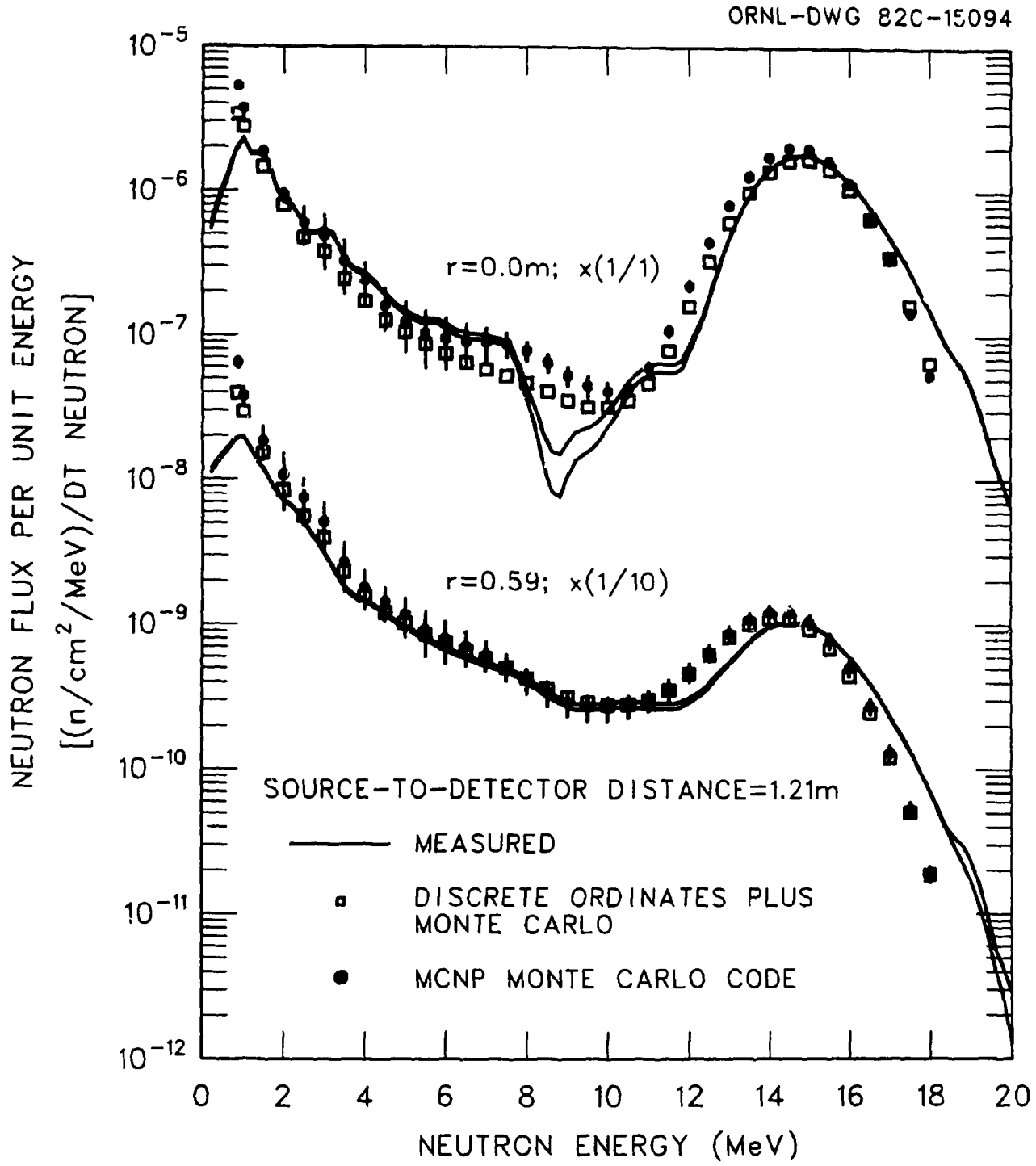

Fig. 3. Neutron flux per unit energy versus neutron energy for the detector at a distance along the z-axis of 1.21 m and at radial distances of 0.0 and 0.59 m from the axis.

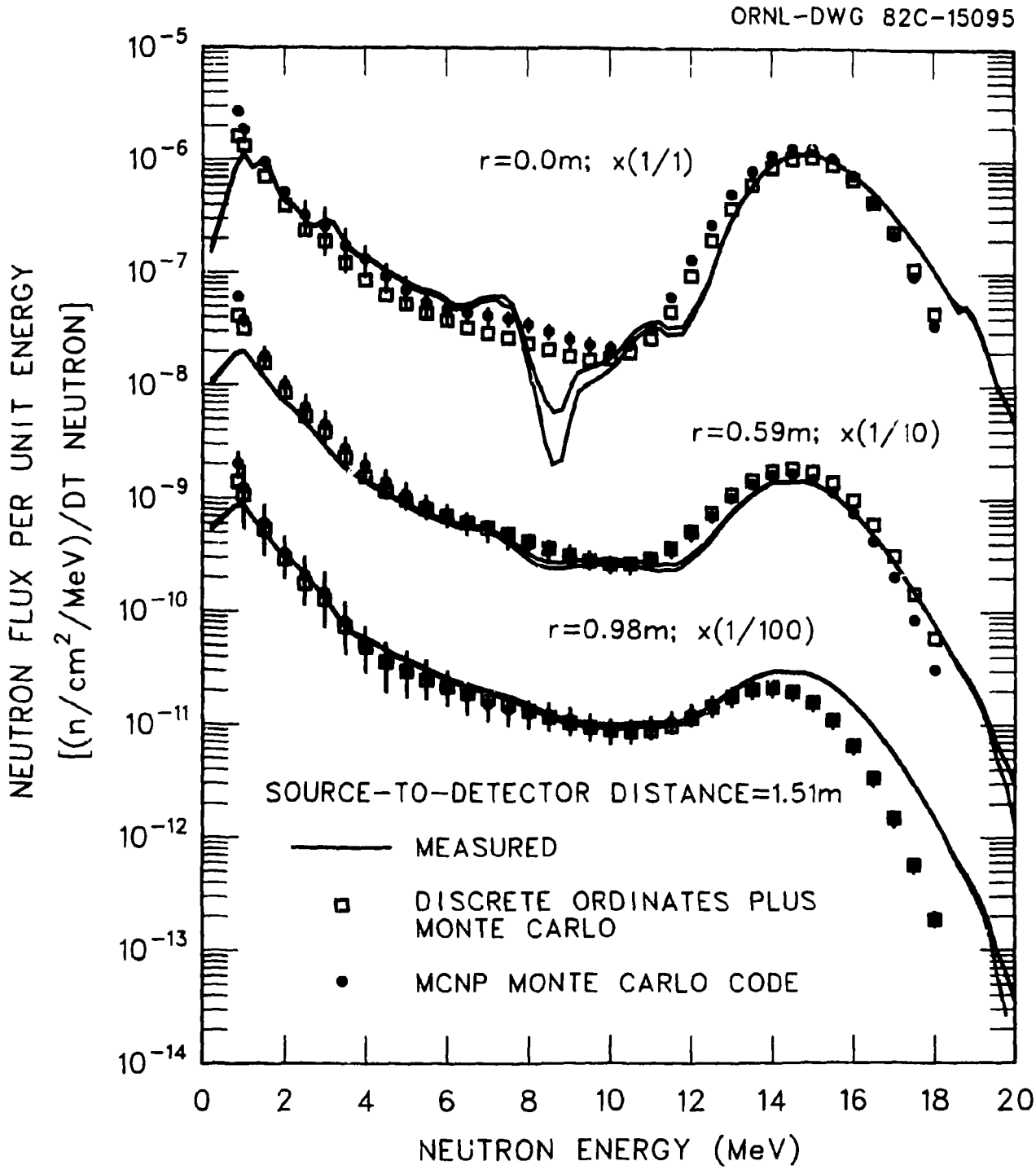

Fig. 4. Neutron flux per unit energy versus neutron energy for the detector at a distance along the z-axis of 1.51 m and at radial distances of 0.0, 0.59, and 0.98 m from the axis.

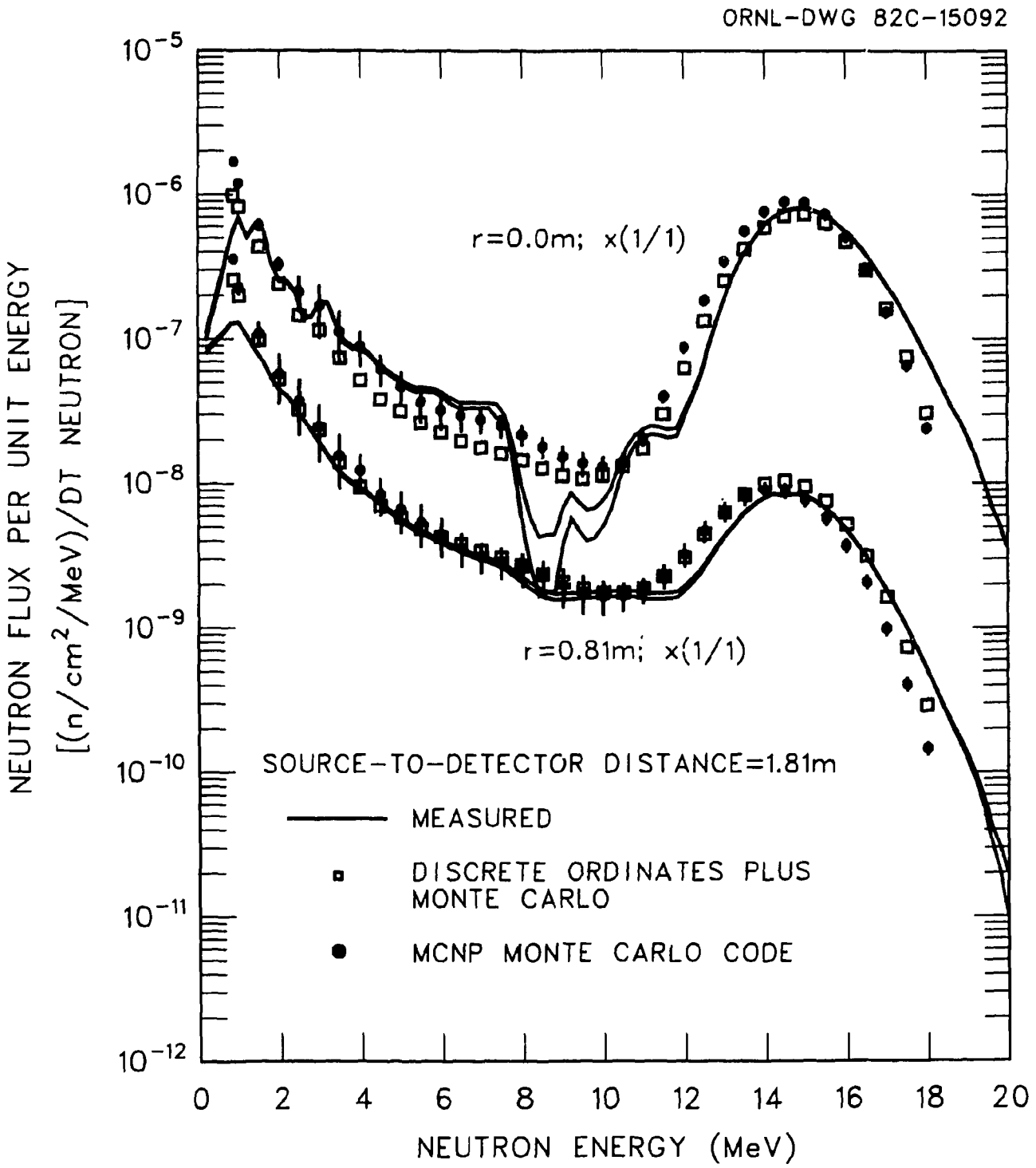

Fig. 5. Neutron flux per unit energy versus neutron energy for the detector at a distance along the z-axis of 1.81 m and at radial distances of 0.0 and 0.81 m from the axis.

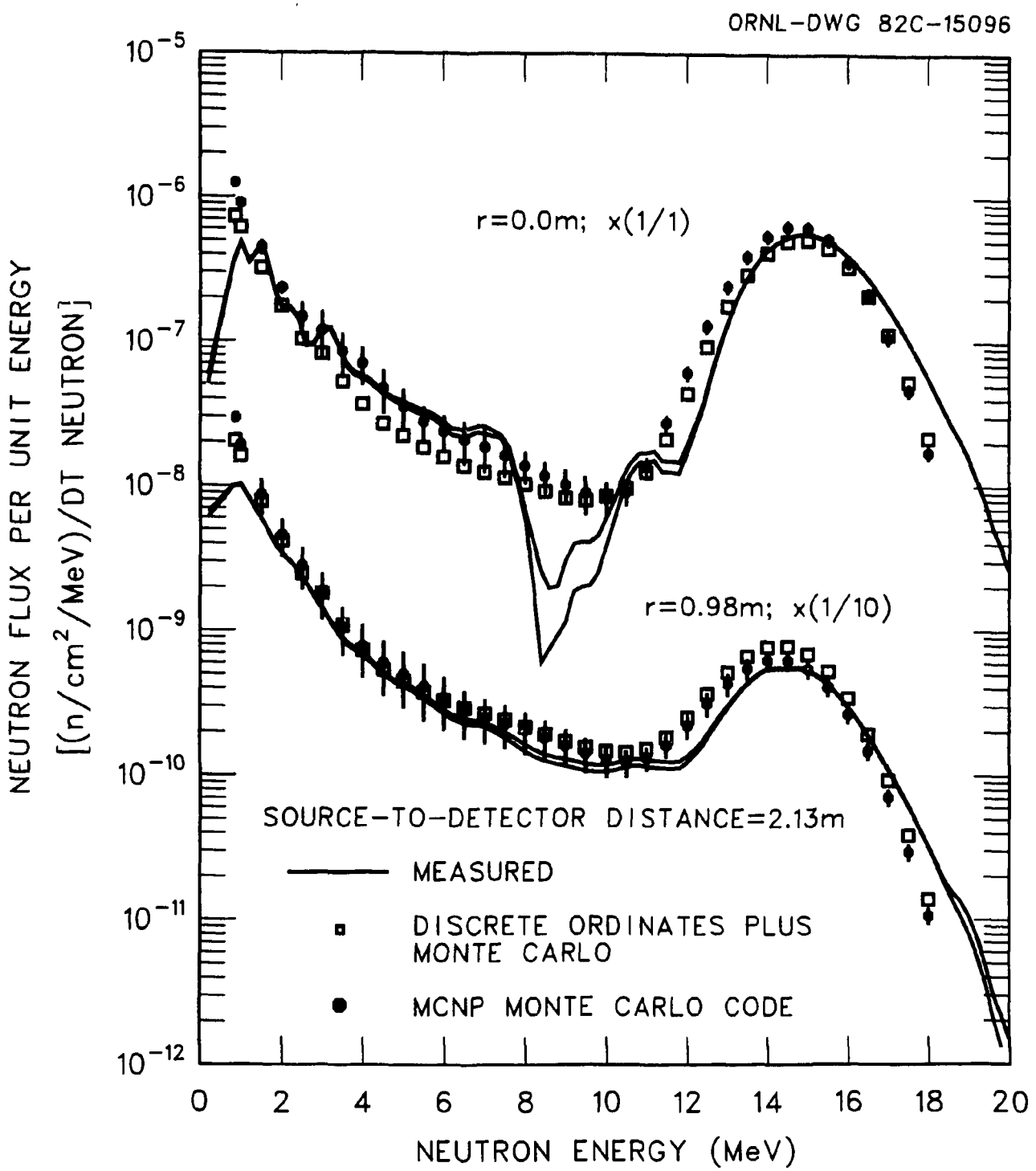

Fig. 6. Neutron flux per unit energy versus neutron energy for the detector at a distance along the z-axis of 2.13 m and at radial distances of 0.0 and 0.98 m from the axis.

Table III

Detector Coordinates

Detector Number	Detector Coordinates (m)			Neutron	Gamma-Ray
	source-to-detector distance along z	r	z[a]		
1	0.94	0.0	1.51	x	
2	0.94	0.39	1.51	x	
3	0.94	0.59	1.51	x	
4	1.21	0.0	1.78	x	
5	1.21	0.59	1.78	x	
6	1.51	0.0	2.08	x	x
7	1.51	0.59	2.08	x	
8	1.51	0.98	2.08	x	x
9	1.81	0.0	2.38	x	
10	1.81	0.81	2.38	x	
11	2.13	0.0	2.70	x	x
12	2.13	0.98	2.70	x	x

[a]z coordinate in Fig. 1.

the duct axis, r = 0.0 m, the MCNP data agree with the measured data particularly well between 850 keV and 8 MeV and reproduce the measurement more closely than the results from Ref. 9. At neutron energies between 8 and 10 MeV, the MCNP calculation overpredicts both the measured and the previously calculated data. However, in this energy range, the measured data exhibit large uncertainties. When the detector is on the axis, the uncollided neutrons dominate the spectrum and the uncollided-to-collided neutron flux ratio above 10 MeV is large. An optimum unfolding of the pulse-height spectrum should yield a high-energy neutron peak that is well separated from the low-energy neutron tail. The broad resolution of the detector combined with the differential nonlinearity introduced by the detector electronics "smear" the pulse-height data and the unfolding code[17] has difficulty in isolating the high- and low-energy components in the spectrum.

At neutron energies above 10 MeV, the MCNP calculations are higher than the measured data between 10 and 14 MeV, in good agreement between 14 and ~15.5 MeV, and then exhibit a more rapid roll-off with increasing neutron energy than the measured data.

The measured and calculated neutron energy spectra are compared at eight detector locations off the axis of the duct, r > 0.0. The spectra are compared at the detector positions where the data calculated in Ref. 9 using only discrete ordinates methods showed the most disagreement with the measured data and where the combined discrete ordinates plus Monte Carlo calculations yielded the most improvement in the agreement between measurement and calculation. Calculating the spectra at these detector positions with the MCNP code offers a fairly stringent test for the code in accounting for the single scattering of neutrons from the duct to the detectors.

The neutron energy spectra calculated at the off-axis detector locations are in good agreement with the measured spectra and those calculated in Ref. 9. All of the data agree to within better than 30% in the neutron energy range between 850 keV and ~12 MeV at all of the detector locations. At neutron energies above 12 MeV, the MCNP results are generally in favorable agreement with the measured and previously calculated data at all of the detector locations. For the detector at r = 0.59 m, in Fig. 2, the MCNP results are in somewhat better agreement with the measured data than the results from Ref. 9. For the detector at r = 0.98 m, in Fig. 4, the MCNP calculation yields identically the same results as the analysis in Ref. 9 at neutron energies above 13 MeV and both calculated spectra are significantly lower than the measured spectra. For the detector at r = 0.98 m, in Fig. 6, the MCNP data underestimate the measured data as well as those from Ref. 9. Some of the disagreement among the data at these detector locations may be due to the angular distributions for elastic scattering in the cross section data. The MCNP calculations were performed using ENDF/B-V cross sections while those in Ref. 9 were made using ENDF/B-IV data. The effects of scattering on the response of the detectors are dominated by the iron duct and for iron there is no difference between the ENDF/B-IV and -V data. The differences between the calculated results at these detector locations may be introduced by the radiation transport procedures.

The measured and calculated energy integrated spectra are compared in Figs. 7-11. These data were obtained by integrating the differential neutron spectra shown in Figs. 2-6 over neutron energy. The MCNP data agree with the measured data to within ~10% in the energy range between 850 keV and 15 MeV for those cases where the detector is on the duct axis. For the off-axis detector positions, the data from MCNP agree with the measured data within ~25%, depending on neutron energy at all detector locations except at r = 0.59 m, Fig. 9, where the disagreement is considerably poorer due to the failure of the calculation to reproduce the high energy peak in the differential spectrum.

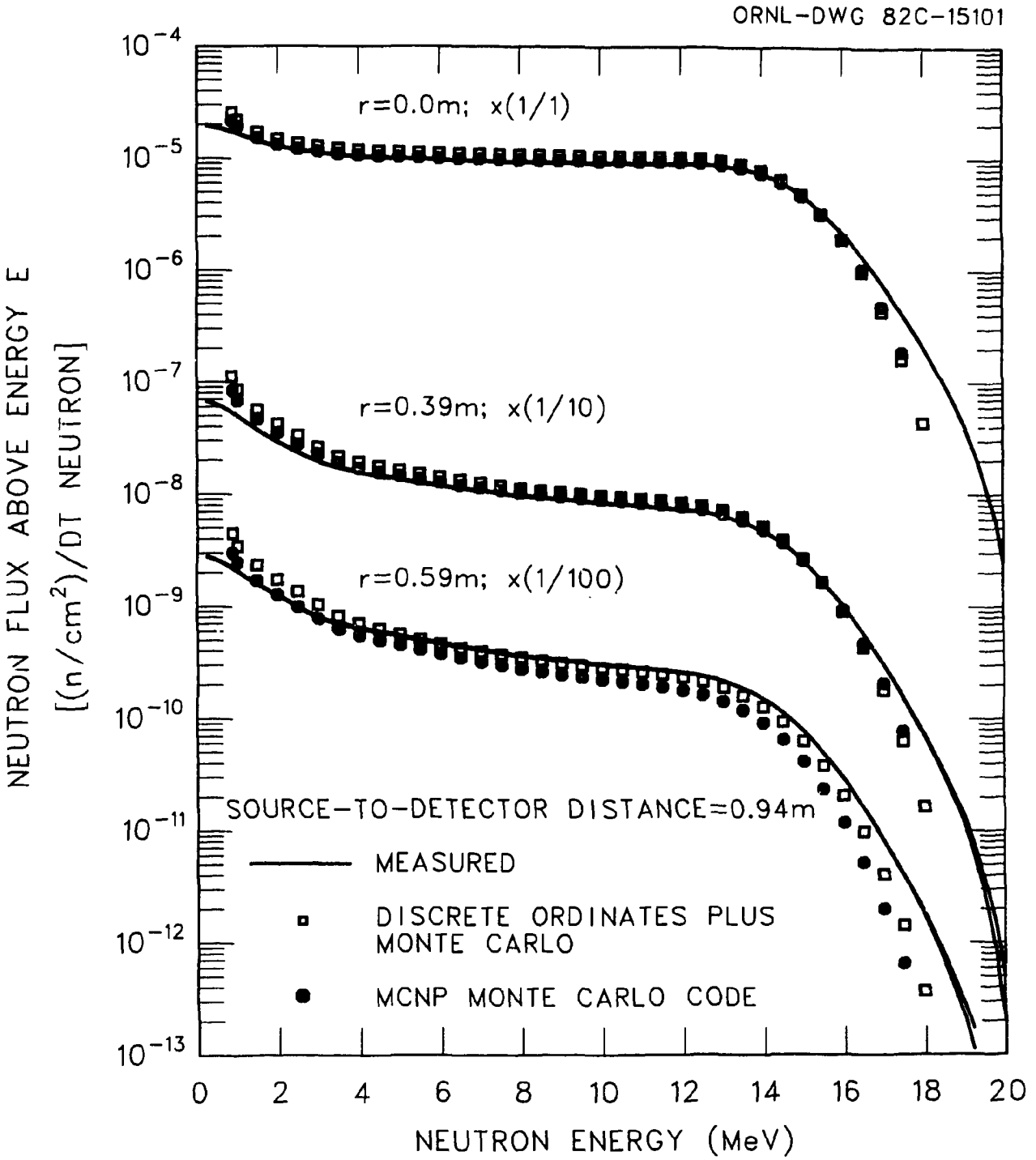

Fig. 7. Neutron flux above energy E versus neutron energy for the detector at a distance along the z-axis of 0.94 m and at radial distances of 0.0, 0.39, and 0.59 m from the axis.

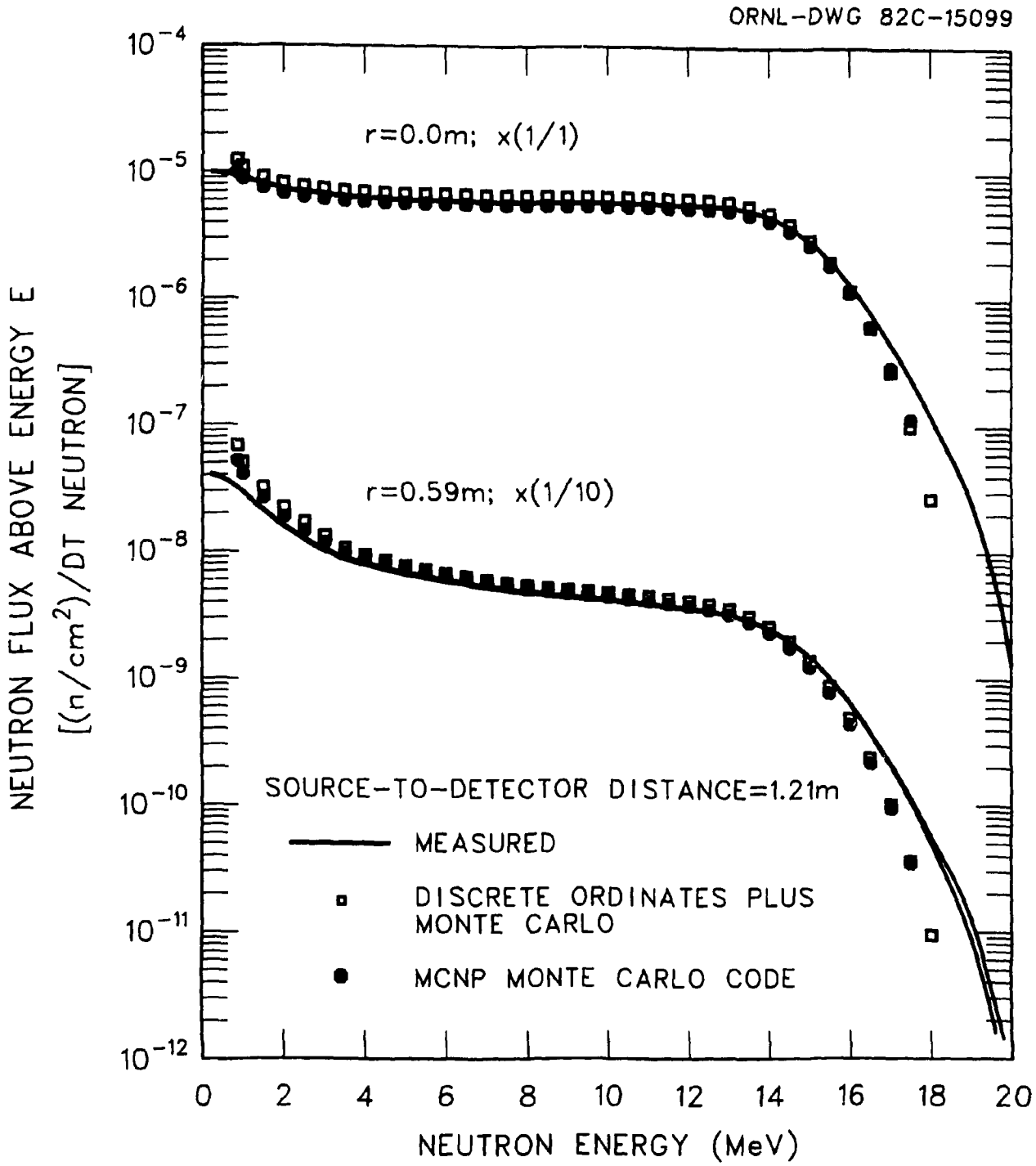

Fig. 8. Neutron flux above energy E versus neutron energy for the detector at a distance along the z-axis of 1.21 m and at radial distances of 0.0 and 0.59 m from the axis.

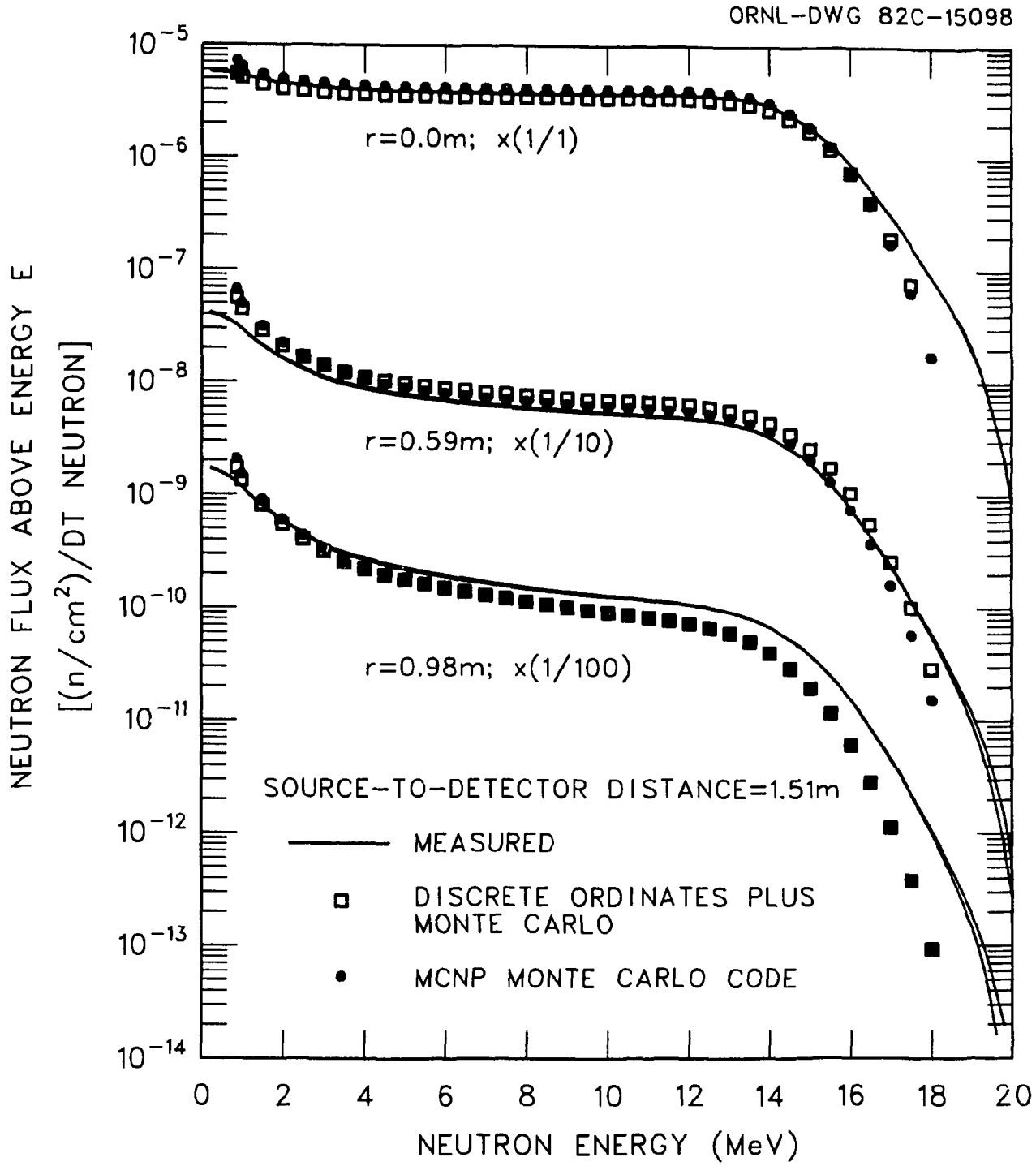

Fig. 9. Neutron flux above energy E versus neutron energy for the detector at a distance along the z-axis of 1.51 m and at radial distances of 0.0, 0.59, and 0.98 m from the axis.

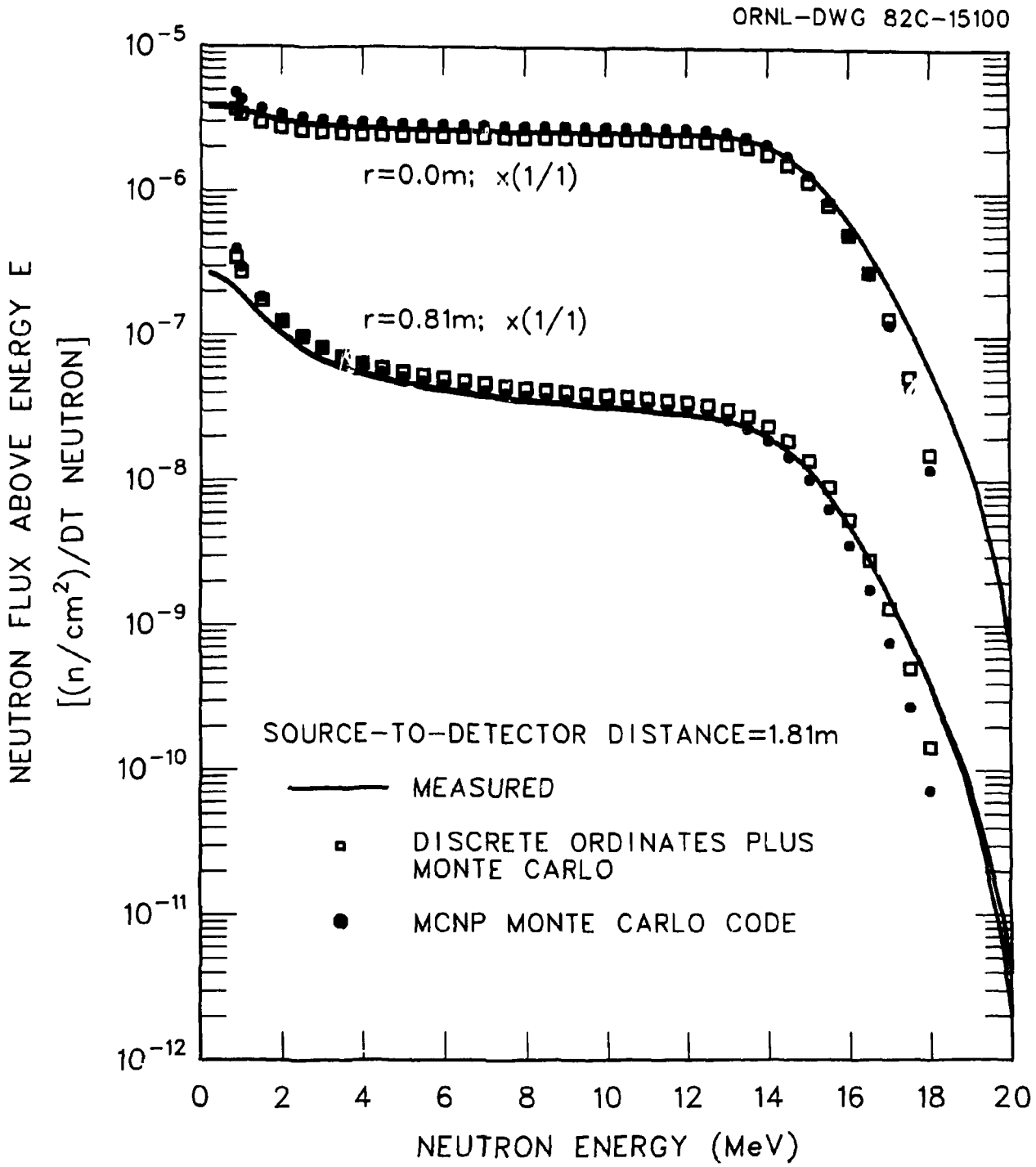

Fig. 10. Neutron flux above energy E versus neutron energy for the detector at a distance along the z-axis of 1.81 and at radial distances of 0.0 and 0.81 m from the axis.

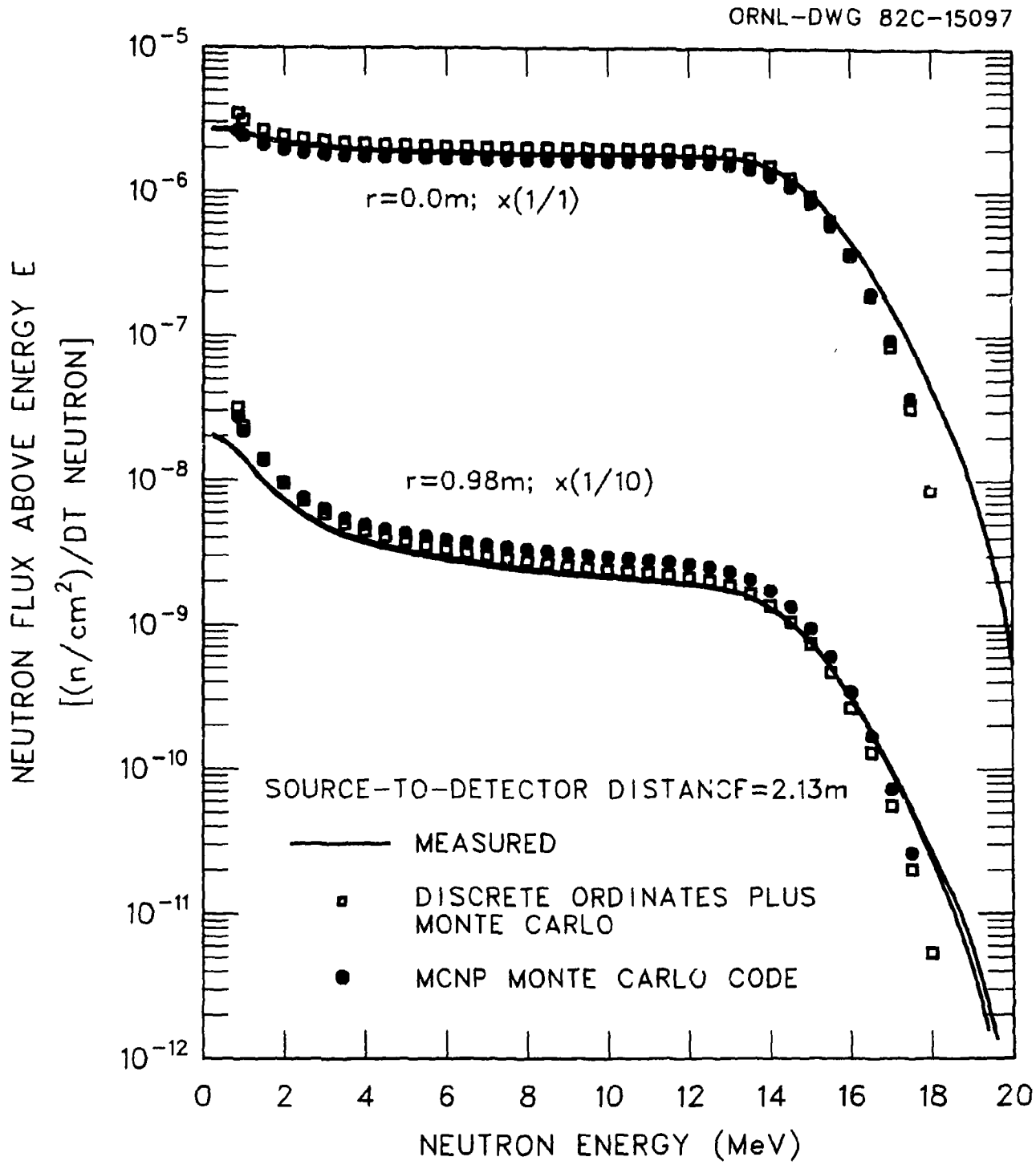

Fig. 11. Neutron flux above energy E versus neutron energy for the detector at a distance along the z-axis of 2.13 m and at radial distances of 0.0 and 0.98 m from the axis.

The differential and integral gamma-ray energy spectra calculated using the MCNP code are compared with the measured spectra and those calculated in Ref. 9 in Figs. 12-15. The calculated gamma-ray spectra were obtained by smoothing the gamma-ray flux per unit energy in each energy interval into which the data were binned with an energy-dependent Gaussian response function having a width determined from

$$R_\gamma = [170 + 288/E_\gamma]^{1/2} \quad (6)$$

where R_γ is the full width at half-maximum of the NE-213 detector resolution to gamma rays of energy E_γ. The gamma-ray flux was binned into twenty-one energy intervals having the same widths as those used in the photon transport in Ref. 9. The calculated gamma-ray energy spectra are compared with the measured data and those from Ref. 9 at only four detector locations. It is assumed that similar agreement among the data would be achieved at the remaining detector locations and that the capability of the MCNP code in reproducing the measured gamma-ray spectra is demonstrated in the comparisons given here.

The gamma-ray spectra obtained using MCNP reproduces the measurements in the energy range between 750 keV and ~10 MeV at all four detector locations. The magnitude of the flux per unit energy is reproduced within better than a factor of two at all energies. Since the flux calculated in MCNP was binned in rather coarse energy intervals, the structure in the measured data are not well reproduced. The MCNP data are also in good agreement (generally within statistics) with the spectra calculated in Ref. 9.

The calculated integral data, shown in Figs. 14 and 15, are in good agreement with the measured and previously calculated spectra at all of the detector locations except at r = 0.98 m, in Fig. 15, where the MCNP results are lower than these data in the energy range between ~1 and ~7 MeV. Otherwise, the data more closely reproduce the measured results.

CONCLUSIONS

The agreement between measured and calculated data obtained in this study suggest that Monte Carlo radiation transport methods that utilize continuous cross section data and appropriate sampling from angular distribution data to account for elastic and inelastic neutron scattering will provide a useful tool for the analysis of 14-MeV neutrons streaming for fusion reactors and related studies. Although Monte Carlo methods have the inherent disadvantage of calculations of nuclear responses at specific locations in a given geometry, compared to determination of the responses throughout the geometry mesh as provided by discrete ordinates techniques, the advantages of accounting for single neutron scattering by the incorporation of continuous cross section data is apparent. In addition, the analysis can be accomplished in a single calculation rather than in a network of codes as in Ref. 9 with the concomittant reduction in computer running times and data management.

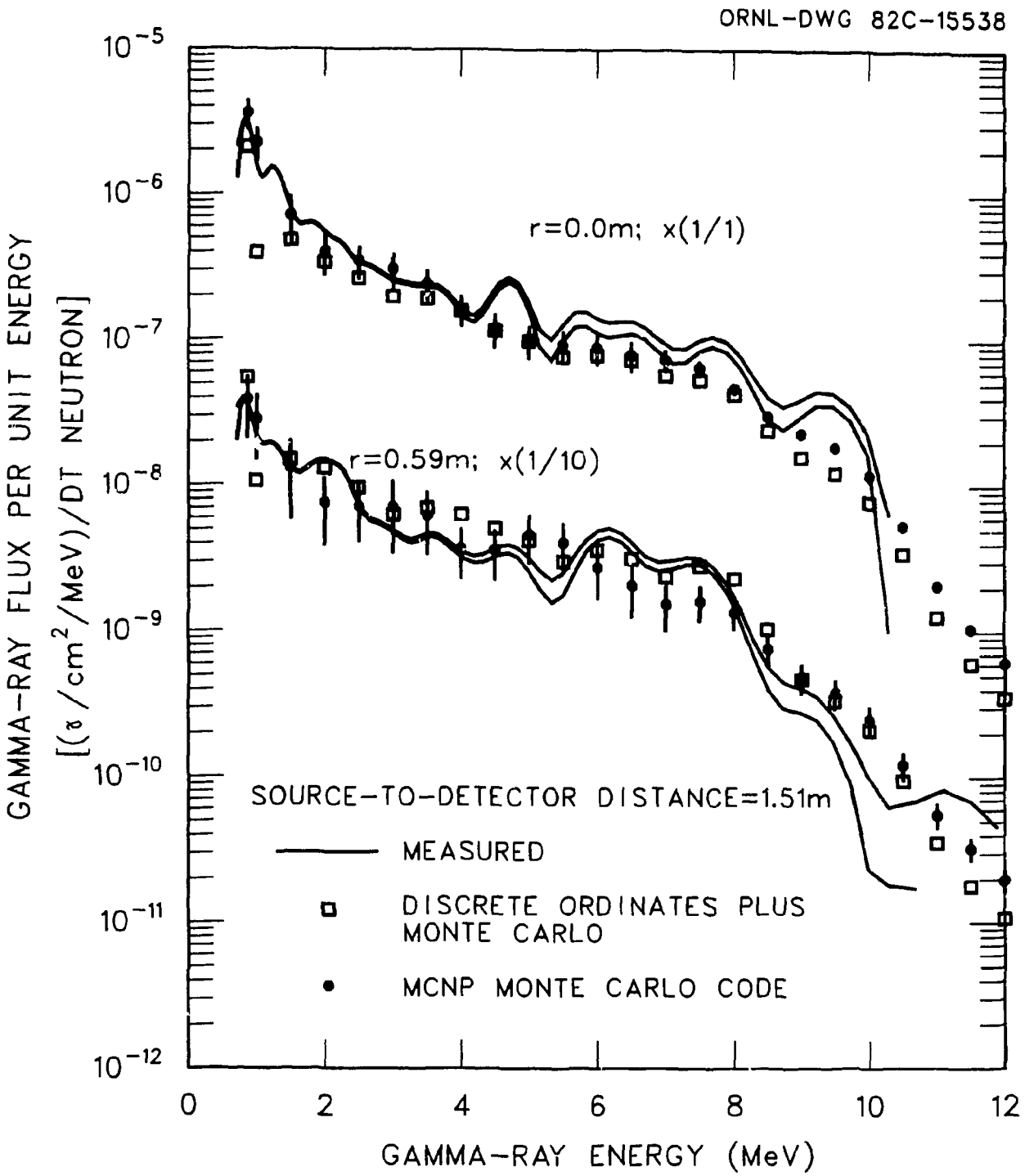

Fig. 12. Gamma-ray flux per unit energy versus gamma-ray energy for the detector at a distance along the z-axis of 1.51 m and at radial distances of 0.0 and 0.59 m from the axis.

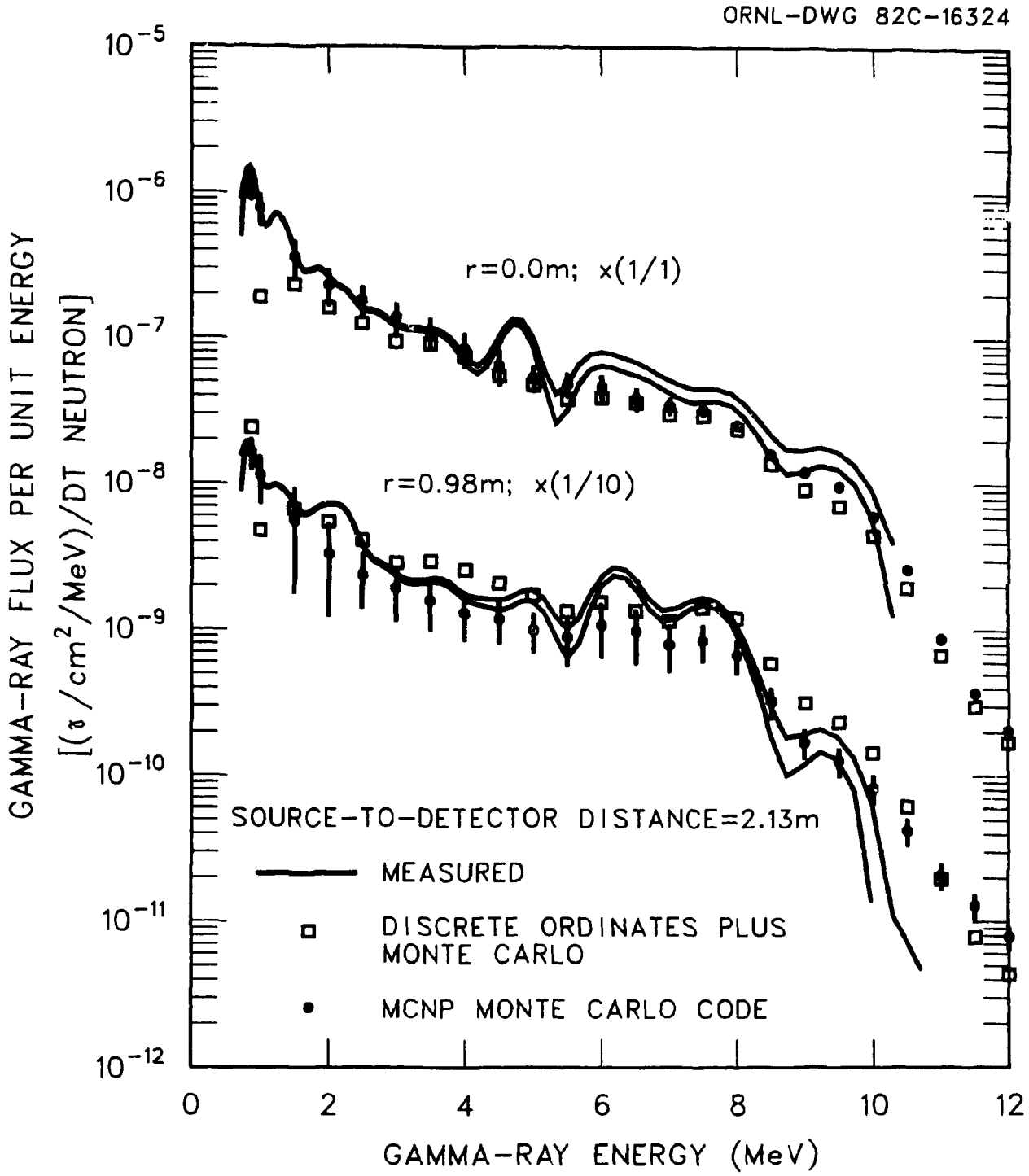

Fig. 13. Gamma-ray flux per unit energy versus gamma-ray energy for the detector at a distance along the z-axis of 2.13 m and at radial distances of 0.0 and 0.98 m from the axis.

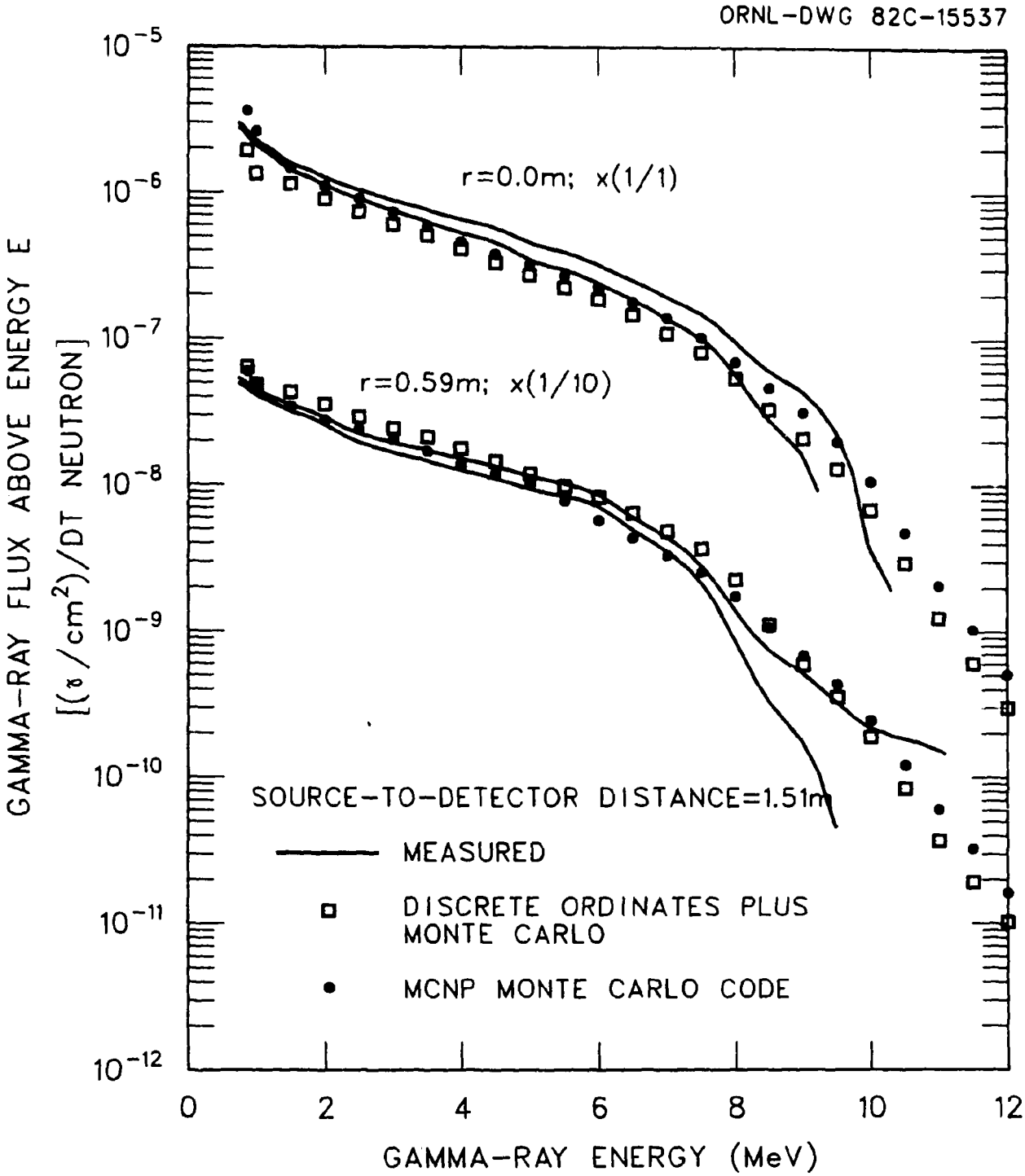

Fig. 14. Gamma-ray flux above energy E versus gamma-ray energy for the detector at a distance along the z-axis of 1.51 m and at radial distances of 0.0, 0.59, and 0.98 m from the axis.

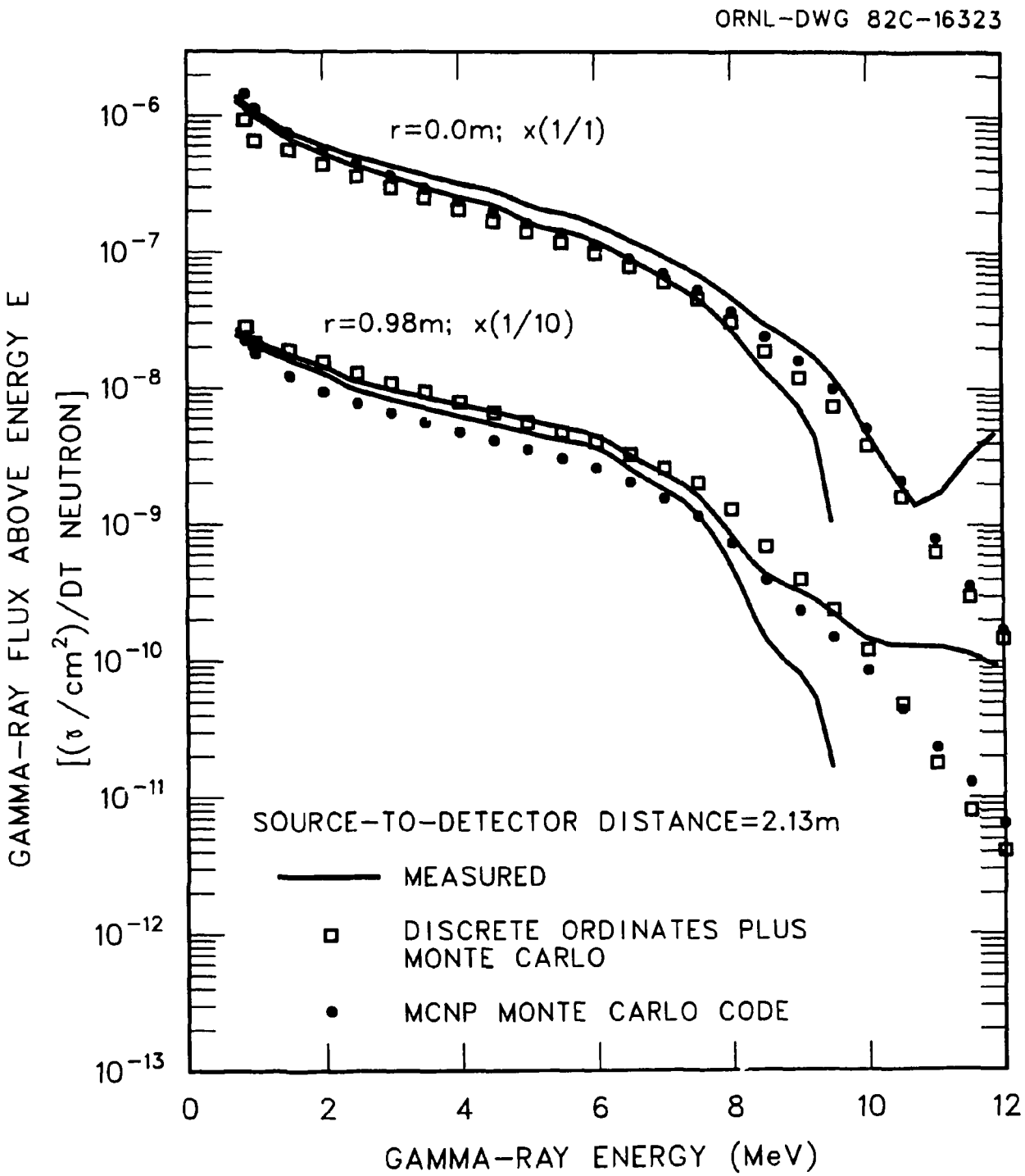

Fig. 15. Gamma-ray flux above energy E versus gamma-ray energy for the detector at a distance along the z-axis of 2.13 m and at radial distances of 0.0 and 0.98 m from the axis.

REFERENCES

1. R. T. Santoro, R. A. Lillie, R. G. Alsmiller, Jr., J. M. Barnes, Nucl. Sci. Eng. *70*, 225 (1979).
2. R. T. Santoro, J. S. Tang, R. G. Alsmiller, Jr., J. M. Barnes, Nucl. Technol. *37*, 65 (1978).
3. M. A. Abdou, L. J. Milton, J. C. Jung, E. M. Gelbard, "Multidimensional Neutronics Analysis of Major Penetrations in Tokamaks," Proc. 2nd Topl. Mtg. Technology of Controlled Nuclear Fusion, Richland, Washington, September 21-23, 1975, Vol. I, p. 845, U.S. Energy Research and Development (1976).
4. W. T. Urban, T. J. Seed, D. J. Dudziak, "Nucleonic Analysis of a Preliminary Design for the ETF Neutral Beam Injector Duct Shielding," Proc. 4th Topl. Mtg. Technology of Controlled Nuclear Fusion," King of Prussia, Pennsylvania, October 14-17, 1980, U.S. Department of Energy (1981).
5. R. A. Lillie, R. T. Santoro, R. G. Alsmiller, Jr., J. M. Barnes, "Neutron and Gamma-Ray Streaming Calculations for the ETF Neutral Beam Injectors," ORNL/TM-7705, Oak Ridge National Laboratory (1981).
6. Y. Seki, H. Iida, R. T. Santoro, H. Kawasaki, M. Yamauchi, Nucl. Technol./Fusion *2*, 272 (1982).
7. M. A. Abdou, Y. Gohar, J. C. Jung, Trans. Am. Nucl. Soc. *38*, 553 (1981).
8. "MCNP - A General Purpose Monte Carlo Code for Neutron and Photon Transport," LA-7396-M (Rev) Version 2B, Los Alamos Monte Carlo Group, Los Alamos National Laboratory (1981).
9. R. T. Santoro, R. G. Alsmiller, Jr., J. M. Barnes, G. T. Chapman, J. S. Tang, Nucl. Sci. Eng. *80*, 586 (1982).
10. R. A. Lillie, R. G. Alsmiller, Jr., J. T. Mihalczo, Nucl. Technol. *43*, 373 (1979).
11. W. A. Rhoades and F. R. Mynatt, "The DOT-III Two-Dimensional Discrete Ordinates Radiation Transport Code," ORNL/TM-4280, Oak Ridge National Laboratory (1979).
12. "FALSTF, Informal Notes," CCC-351, Radiation Shielding Information Center, Oak Ridge National Laboratory (1979).
13. R. W. Roussin, C. R. Weisbin, J. E. White, N. M. Greene, R. Q. Wright, J. B. Wright, "Processed Multigroup Cross Section Library for Neutronics Studies," ORNL/RSIC-37, Radiation Shielding Information Center, Oak Ridge National Laboratory (1975); also available from RSIC as Data Library Collection, DLC-41.
14. M. M. Waddel, Jr., "PXMORSE, A Continuous Energy Monte Carlo Code," Ph.D. Thesis, University of Tennessee (1981).
15. R. T. Santoro, J. M. Barnes, R. G. Alsmiller, Jr., E. M. Oblow, "Calculational Procedures for the Analysis of Integral Experiments for Fusion Reactor Design: Attenuation Experiments," ORNL-5777, Oak Ridge National Laboratory (1981).
16. G. T. Chapman, G. L. Morgan, J. W. McConnell, "The ORNL Integral Experiments to Provide Data for Evaluating MFE Shielding Concepts. Part I: Attenuation Measurements," ORNL/TM-7356.
17. W. R. Burrus and V. V. Verbinski, Nucl. Instrum. Methods *67*, 181 (1979).